

# *Preliminary Experimental Verification of Self-Excited Wound-Field Synchronous Motor with Auxiliary Poles for Automotive Applications*

Masahiro Aoyama

Department of Environment and Energy System,  
Graduate School of Science and Technology,  
Shizuoka University / SUZUKI motor corporation  
300 Takatsuka-cho, Minami-ku, Hamamatsu,  
Shizuoka 432-8611, Japan  
aoyamam@hhq.suzuki.co.jp

Toshihiko Noguchi

Department of Electrical and Electronics Engineering,  
Graduate School of Engineering,  
Shizuoka University  
3-5-1 Johoku, Naka-ku, Hamamatsu,  
Shizuoka 432-8561, Japan  
tnogut@ipc.shizuoka.ac.jp

**Abstract**—This paper describes a rare-earth-free synchronous motor where space harmonic power is utilized for field magnetization instead of permanent magnets for automotive applications. The stator has a concentrated winding structure, and the rotor has separate two types of windings, i.e., an induction coil that retrieves mainly the second space harmonic and an excitation coil for the field magnetization. The two coils are connected via a center-tapped full bridge diode rectifying circuit. The theoretical analysis is conducted, and the mechanical configuration is discussed. In addition, preliminary experimental test result is demonstrated from the viewpoint of the principle of self-excitation.

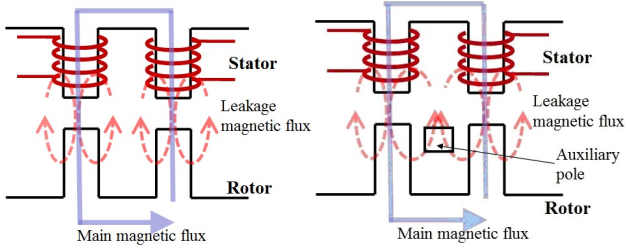
**Keywords**—synchronous motor; self-excitation; wound-field; space harmonics; induced current; rare-earth-free; electric vehicle.

## I. INTRODUCTION

Recently, various technical portfolios are considered, e.g., low-end hybrid system based on a 12-V idling stop system, and a high-efficiency power train technology with a high electrification ratio to achieve zero-emission. Regarding an electric-machine as an energy conversion device, an Interior Permanent Magnet Synchronous Motor (IPMSM) is commonly applied to Hybrid Vehicles (HEVs) and Electric Vehicles (EVs) because of its high efficiency [1]. Permanent magnets used for the IPM motor are, however, very expensive because Nd-Fe-B magnets are generally employed to achieve higher energy density and to improve fuel efficiency at low-load operation for street use. Moreover, the traction motors are usually installed on the chassis, where special countermeasures must be taken from the viewpoints of environmental and thermal issues. In order to restrain demagnetization caused by the temperature rise of the permanent magnets for example, expensive rare-earth metals such as Dy and Tb must be added to the Nd-Fe-B magnets. A material technology development, which is intensively placed Dy and Tb where the demagnetizing point easily, is actively engaged. However, a global maldistribution problem of the natural resources such as Dy and Tb is not discussed.

Therefore, varieties of rare-earth-free motors, particularly wound-field synchronous motors which replaces magnets with electromagnets are focused on due to the remarkable rise of the Nd-Fe-B magnet market price [2][3]. These separate-excited wound-field machines, i.e., the wound-field flux switching motor has advantage in terms of a robust rotor structure for high-speed operation. The great merit of the high-speed operation is to reduce the weight of the machine. The torque density of these motors is, however, lower than that of IPMSM because it cannot utilize reluctance torque but only electromagnet torque which is generated by the DC field excitation.

Recently, the self-excited wound-field synchronous motor that utilizes the space harmonics for the field magnetization has been studied in the industries for the automotive traction application [4]-[15]. The classic self-excitation is roughly classified into three types. The former has an additional auxiliary windings on the primary side for space harmonics generation utilizing self-excitation [4]-[11]. The second excites the armature windings with time harmonic injection, habitually [12][13]. The third, however, can eliminate these auxiliary windings or time harmonic injection, because the space harmonics for the self-excitation can be obtained by the concentrated winding structure [14]-[17]. In addition, the third one has potential to obtain a position of the post IPMSM by achieving the comparable torque density with the rare-earth-free configuration. Because it can utilize the reluctance torque and the self-excited electromagnet torque without additional space harmonic excitation windings in the stator slots. In the past works [14]-[17], however, it cannot efficiently retrieve the space harmonics power. The authors already proposed a rare-earth-free motor utilizing effectively the space harmonics for the field magnetization power [18]-[20]. This proposed motor is the same self-excitation principle, but, it can efficiently retrieve the space harmonics by placing auxiliary poles on the  $q$ -axis. Figure 1 shows a simplified salient pole model of the motor. As can be seen in the figure, the proposed model in [18]-[20] can improve the stator-rotor coupling coefficient of the leakage magnetic flux



(a) Benchmark model. (b) Proposed model.  
Fig. 1. Main magnetic path and leakage magnetic path.

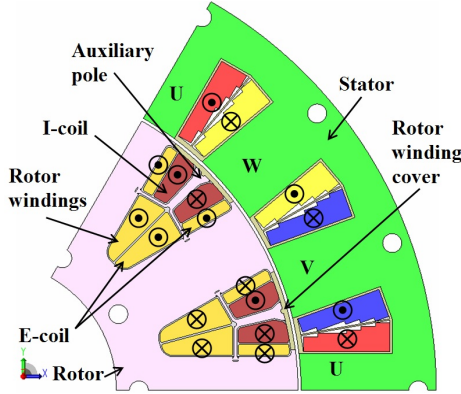


Fig. 2. Cross section of proposed motor.

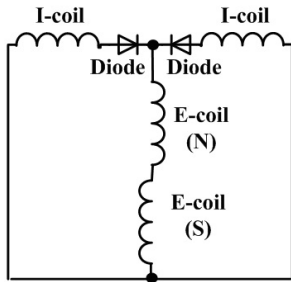


Fig. 3. Rotor winding connection using full-bridge rectifier.

TABLE I. SPECIFICATIONS OF MOTOR.

Number of rotor poles	12
Number of stator slots	18
Stator outer diameter	200 mm
Rotor diameter	138.6 mm
Axial length of core	108 mm
Air gap length	0.7 mm
Armature magnetomotive force	1686 $A_{rms}T$
Number of I-pole coil-turn	53 T
Number of E-pole coil turn	122 T
Thickness of iron core steel plate	0.30 mm (30DH)

by the effect of auxiliary poles compared with the benchmark model presented in [15]-[17]. The electromagnet torque caused by the space harmonics and the reluctance torque

caused by the saliency are simultaneously delivered in the proposed motor, but the electromagnet torque generated by the auxiliary poles and the salient poles on the rotor takes a significant part of the total torque. Because the reduction of the induced voltage in the rotor windings of the self-excited wound-field motor is hard to avoid in the low speed range, the strong stator-rotor coupling coefficient of the leakage magnetic flux which generates the electromagnet torque is significantly important. The additional torque can be increased by placing the auxiliary poles on the  $q$ -axis, where the space harmonic magnetic flux can be retrieved effectively.

In this paper, a theoretical discussion of the proposed motor is conducted. Second, the mechanical design are summarized. Proposed motor is designed as a traction motor for B-segment hybrid electric vehicles. In addition, the preliminary experimental test result is demonstrated from the viewpoint of the principle of the self-excitation.

## II. CONFIGURATION AND SPECIFICATIONS OF PROPOSED MOTOR

Figure 2 shows a cross section of the proposed motor where the wound-field coils are installed to the rotor salient poles, and the induction coils are placed in spaces between the rotor salient poles, i.e., rotor slots. Conventional common motors such as a synchronous reluctance motor (SynRM) dissipate the space harmonics power caused by the stator with the concentrated winding structure, whereas the proposed motor positively takes advantage of the space harmonics power for the field magnetization. Each of the induction poles (I-pole) is a special pole exclusively used to generate the magnetizing power from the second space harmonics. In addition, it is magnetically independent of the main magnetic flux path to prevent reduction of the saliency ratio. The I-poles, i.e., auxiliary poles, are fitted between the salient poles with wedge form and held from an axial direction using a rotor winding cover. On the other hand, each excitation pole (E-pole) has saliency on the rotor for the field excitation, which uses the retrieved second harmonic power. In addition, E-pole can retrieve the  $d$ -axis space harmonics. The both coils are connected via a diode rectifying circuit as shown in Fig. 3. Specifications of the motor are listed in Table I.

## III. THEORETICAL AND SIMULATION ANALYSIS

### A. Magnetomotive Force of Concentrated Winding

The magnetomotive force generated by the concentrated winding structure has the second-order space harmonic on the fundamental magnetic field. Figure 4(a) shows magnetic flux density waveforms in the air gap, where the distributed winding structure of 12 poles-72 slots (1-to-6-slot-combination) and the concentrated winding structure of 12 poles-18 slots (2-to-3-slot-combination) are compared. Figure 4(b) shows harmonic contents of the magnetic flux density, which is analyzed by Fourier series and a developed formula of Fourier series of Fig. 4(a). As can be seen in Fig. 4, the magnetic flux waveform of the distributed winding structure is basically sinusoidal, except for the slot harmonics. However, the waveform of the concentrated winding structure is

distorted by the second-order harmonic component. The second-order harmonic component is caused because every phase winding is wound separately on an individual tooth without superposition on the other phase windings.

### B. Mathematical Model on $dq$ Reference Frame

The motor with the 2-to-3-slot-combination has a  $d$ -axis inductance composed with a constant part and a periodical third time harmonics part caused by the rotation. Therefore, the  $d$ -axis rotor self-inductance  $L_{rd}$  and the  $q$ -axis rotor self-inductance  $L_{rq}$  can be given by

$$L_{rd}(\omega t) = L_{rd0} + L_{rda} \cos 3\omega t, \quad (1)$$

$$L_{rq}(\omega t) = L_{rq0} + L_{rqa} \cos \left( 3\omega t - \frac{\pi}{6} \right), \quad (2)$$

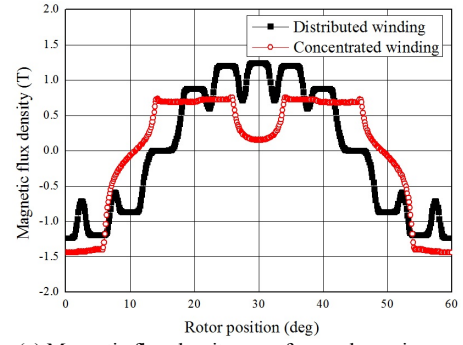
where  $L_{rd0}$  and  $L_{rq0}$  are the constant parts, and  $L_{rda}$  and  $L_{rqa}$  are the amplitudes of the periodical variations [19].  $\omega$  is an electrical synchronous angular velocity. The mathematical model of the proposed motor can be expressed as the following voltage equation:

$$\begin{aligned} \begin{bmatrix} v_{sd} \\ v_{sq} \\ v_{rd} \\ v_{rq} \end{bmatrix} &= \begin{bmatrix} R_s & 0 & 0 & 0 \\ 0 & R_s & 0 & 0 \\ 0 & 0 & R_r & 0 \\ 0 & 0 & 0 & R_r \end{bmatrix} \begin{bmatrix} i_{sd} \\ i_{sq} \\ i_{rd} \\ i_{rq} \end{bmatrix} + \begin{bmatrix} p & -\omega & p & -\omega \\ \omega & p & \omega & p \\ p & 0 & p & 0 \\ 0 & p & 0 & p \end{bmatrix} \begin{bmatrix} \psi_{sd} \\ \psi_{sq} \\ \psi_{rd} \\ \psi_{rq} \end{bmatrix} \\ &= \begin{bmatrix} R_s & 0 & 0 & 0 \\ 0 & R_s & 0 & 0 \\ 0 & 0 & R_r & 0 \\ 0 & 0 & 0 & R_r \end{bmatrix} \begin{bmatrix} i_{sd} \\ i_{sq} \\ i_{rd} \\ i_{rq} \end{bmatrix} + \begin{bmatrix} L_{sd} & 0 & M_d & 0 \\ 0 & L_{sq} & 0 & M_q \\ M_d & 0 & L_{rd} & 0 \\ 0 & M_q & 0 & L_{rq} \end{bmatrix} p \begin{bmatrix} i_{sd} \\ i_{sq} \\ i_{rd} \\ i_{rq} \end{bmatrix}, \\ &\quad + \omega \begin{bmatrix} 0 & -(L_{sq} + M_q) & 0 & -(M_q + L_{rq}) \\ L_{sd} + M_d & 0 & M_d + L_{rd} & 0 \\ 0 & 0 & 0 & 0 \\ 0 & 0 & 0 & 0 \end{bmatrix} \begin{bmatrix} i_{sd} \\ i_{sq} \\ i_{rd} \\ i_{rq} \end{bmatrix} \end{aligned} \quad (3)$$

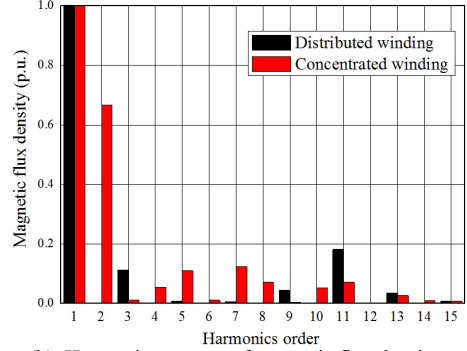
where  $v_{sd}$ ,  $v_{sq}$ ,  $i_{sd}$  and  $i_{sq}$  are the armature voltages and currents,  $v_{rd}$ ,  $v_{rq}$ ,  $i_{rd}$  and  $i_{rq}$  are the  $d$ -axis and  $q$ -axis rotor winding voltages and currents,  $R_s$  and  $R_r$  are the armature winding and rotor winding resistances,  $M_d$  and  $M_q$  are the  $d$ -axis and  $q$ -axis mutual inductances, and  $p$  denotes a differential operator, respectively [19].

The output torque of the proposed motor is obtained by the vector product between the armature current and the magnetic flux, which is associated with the fourth term in Eq. (3):

$$\begin{aligned} T &= P_p \begin{bmatrix} i_{sd} & i_{sq} \end{bmatrix} \begin{bmatrix} 0 & -(L_{sq} + M_q) & 0 & -(M_q + L_{rq}) \\ L_{sd} + M_d & 0 & M_d + L_{rd} & 0 \end{bmatrix} \begin{bmatrix} i_{sd} \\ i_{sq} \\ i_{rd} \\ i_{rq} \end{bmatrix} \\ &= P_p (L_{sd} - L_{sq}) i_{sd} i_{sq} \\ &\quad + P_p \{ (M_d - M_q) i_{sd} i_{sq} - (M_q + L_{rq}) i_{sd} i_{rq} + (M_d + L_{rd}) i_{rd} i_{sq} \} \end{aligned}$$



(a) Magnetic flux density waveforms along air gap.



(b) Harmonic contents of magnetic flux density.

Fig. 4. Magnetic flux density along air gap under no-load.

(4)

where  $P_p$  is the pole-pair number. As expressed in the above expression, the output torque is composed of the two terms, i.e., the reluctance torque and the electromagnet torque. Since the field current generating the electromagnet torque is proportional to  $\omega$ , the benchmark model which is suggested in cannot deliver the sufficient torque in the low-speed range [15]-[17]. However, the proposed model can solve that problem by improving the coupling coefficient between the stator and the rotor, i.e., mutual inductance, which can be seen in the second term of Eq. (4).

### C. Electromagnetic Field Analysis

The effectiveness of setting the auxiliary pole, i.e., I-pole, on the  $q$ -axis and the driving performance can be explicated below by the FEM analysis results with a software JMAG-Designer ver. 13. Figure 5 shows magnetic flux vectors and flux lines of the third time harmonics on the  $dq$  reference frame simulated by the magnetic field analysis. As shown in the figure, the third time harmonic magnetic flux mainly flows through a space between the rotor salient poles, whose direction corresponds to the  $q$ -axis, and leaks to the salient poles on the  $d$ -axis. Therefore, the third time harmonic power can be efficiently retrieved by placing the auxiliary poles on the  $q$ -axis as shown in Fig. 5 (b). Since the model without the auxiliary poles has both of the induction coil and the excitation coil on the same salient pole, which corresponds to the  $d$ -axis, it is rather difficult to retrieve the third time harmonic power efficiently. The wide rotor tooth is required to prevent the magnetic saturation because the salient pole wound by the E-pole winding is magnetized by the field

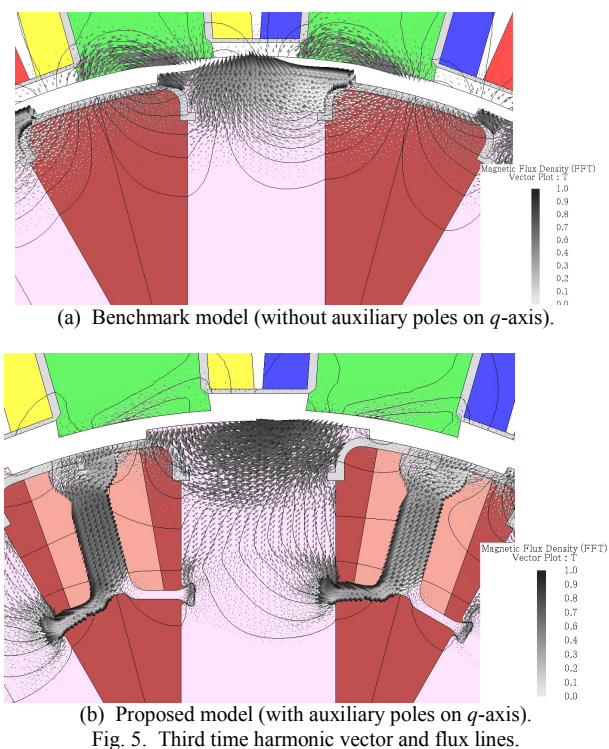
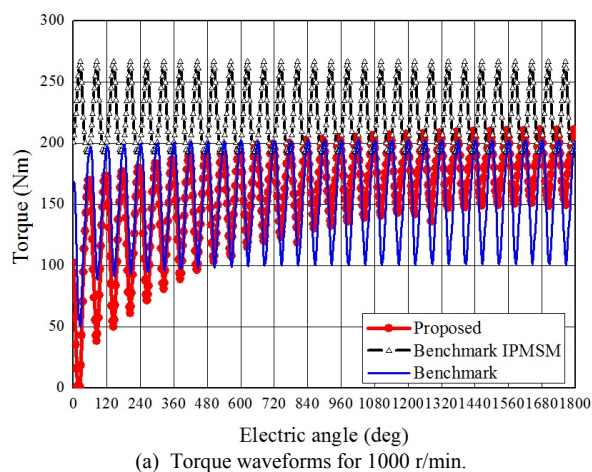
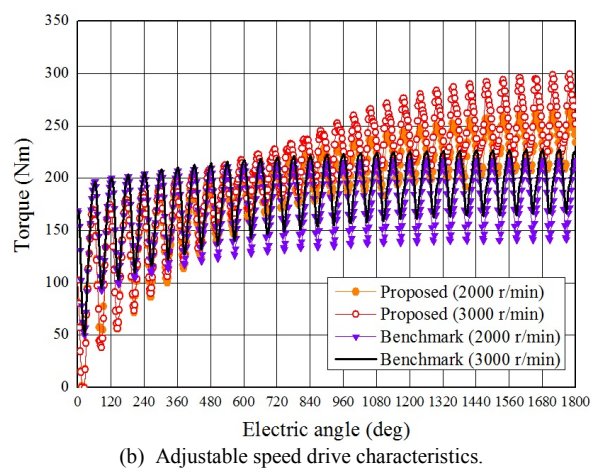


Fig. 5. Third time harmonic vector and flux lines.



(a) Torque waveforms for 1000 r/min.



(b) Adjustable speed drive characteristics.

Fig. 6. Torque waveforms with respect to rotation speed.

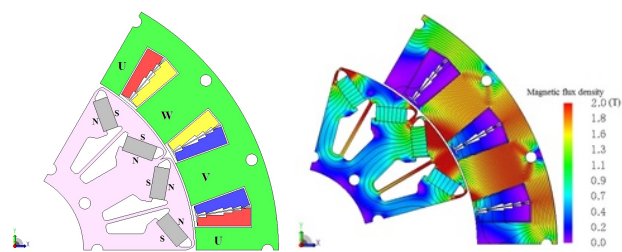


Fig. 7. Cross section of concentrated winding IPMSM.

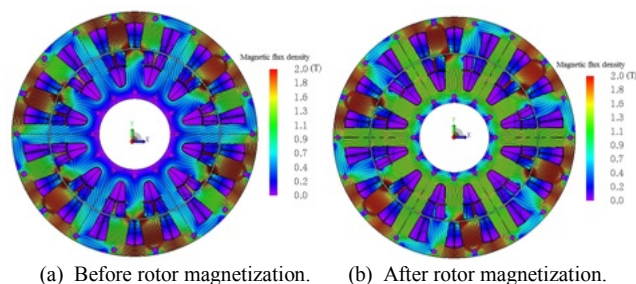


Fig. 8. Magnetic flux density and flux lines for 1000 r/min.

current. However, widening the tooth of the salient pole affects the organization of shorting magnetic path of the third space harmonics as shown in Fig. 5 (a). The model with the auxiliary poles shown in Fig 5 (b), however, has the induction coil and the excitation coil separately on the  $q$ -axis and the  $d$ -axis, respectively, which results in effective retrieval of the third time harmonic power. As shown in Fig. 5 (b), it is confirmed the third time harmonic magnetic flux is orthogonal to the I-pole. Figure 6 shows the torque characteristics of the proposed motor, the benchmark model, and the concentrated winding IPMSM (magnet material:  $B_r=1.22$  T,  $BH_{max}=286$  kJ/m<sup>3</sup> at 300K) shown in Fig. 7, for 1000 r/min by the maximum armature magnetomotive force 1686 A<sub>rms</sub>T under MTPA control calculated by the magnetic field analysis. As shown in Fig. 6, the torque density at 1000 r/min of the proposed motor is 15.4 % lower than that of the IPMSM model, while the proposed motor surpasses the IPMSM at 2000 r/min. On the other hand, the torque density of the benchmark model is 14.2 % lower at 2000 r/min. It can be confirmed that the additional torque generated by the self-excitation using the space harmonic power is significant to satisfy the comparable level of the total output torque as the IPMSM. Furthermore, the advantages of the auxiliary poles are studied, focusing on the torque ripple characteristics. Figure 8 shows a process of the rotor magnetization, which is generated by self-excitation, in the transient state. The electromagnetomotive force in the circumferential direction can be observed in the rotor salient poles after the rotor magnetization is completely formed. However, the low torque density in the extremely low-speed range is difficult to avoid because the amplitude of induced voltage in the rotor windings is based on Faraday's law. Around zero r/min, torque density

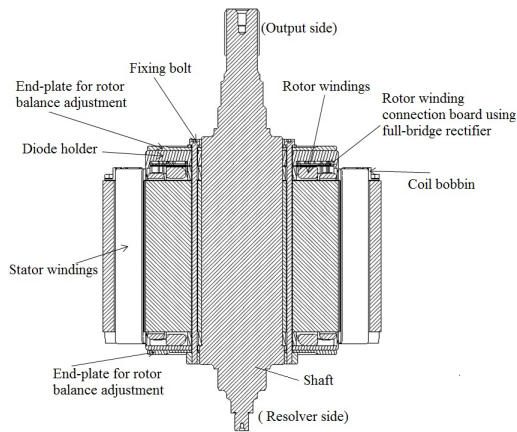


Fig. 9. Mechanical configuration of prototype.



(a) Laminated rotor and stator cores.



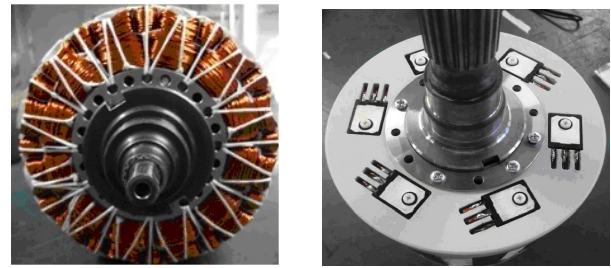
(b) Segmented auxiliary pole.

Fig. 10. Motor cores of prototype.

becomes low, although the high torque density is demanded for the automotive operation particular, e.g., bump ride-over.

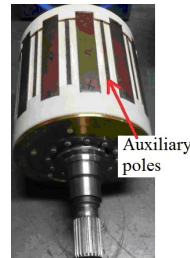
#### IV. PROTOTYPE MACHINE

Figure 9 illustrates a three-dimensional component exploded views of the prototype. Both I-pole and E-pole windings are connected with a printed wire board on the rotor ends as shown in Fig. 9, and the diodes are fixed on the board. Figure 10 shows motor cores of the actual prototype machine. The I-poles, i.e., auxiliary poles, are inserted in the rotor slots with wedge-formed beams, and are held from an axial direction using a rotor winding cover. Figure 11 shows the prototype machine with a proposed self-excited wound-field rotor, a full-bridge rectifier mounted on the rotor windings and a concentrated winding stator.

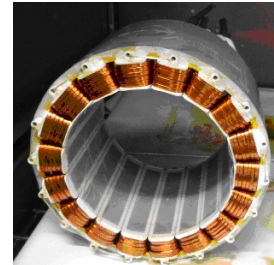


(a) Wound-field rotor.

(b) Full-bridge rectifier.

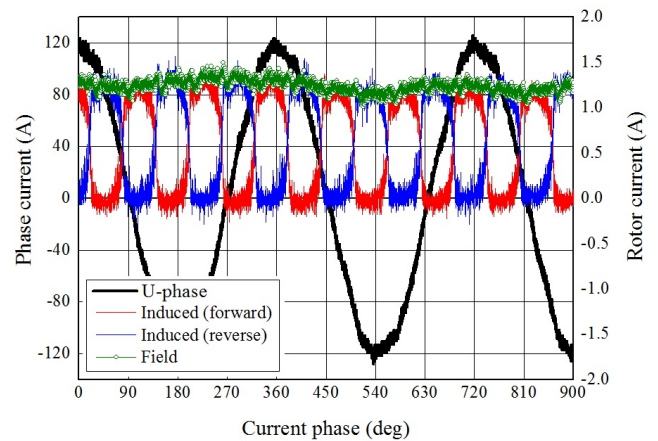


(c) Auxiliary poles.

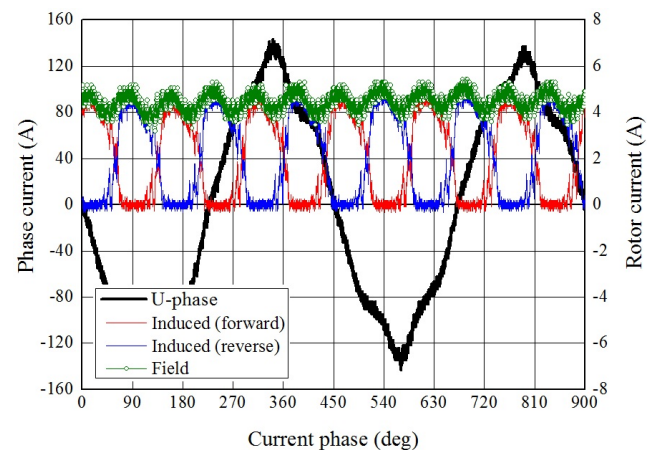


(d) Concentrated winding stator.

Fig. 11. Prototype machine.

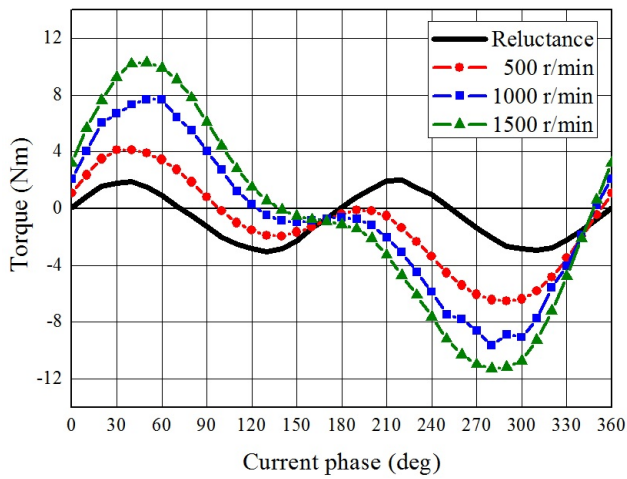


(a) 500 r/min under  $414 A_{rms} T$ .

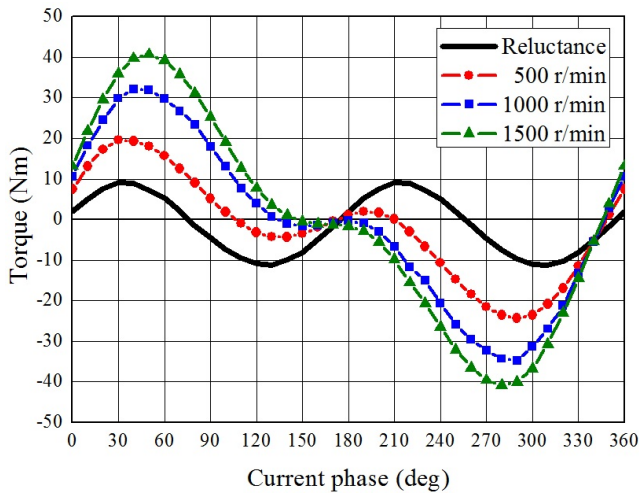


(b) 2000 r/min under  $414 A_{rms} T$ .

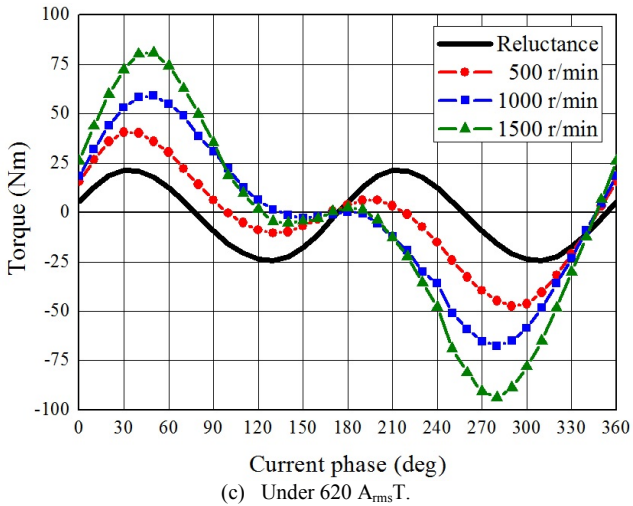
Fig. 12. Stator and rotor current waveforms.



(a) Under 210  $A_{rms}T$ .



(b) Under 414  $A_{rms}T$ .



(c) Under 620  $A_{rms}T$ .

Fig. 13. Adjustable speed drive characteristics.

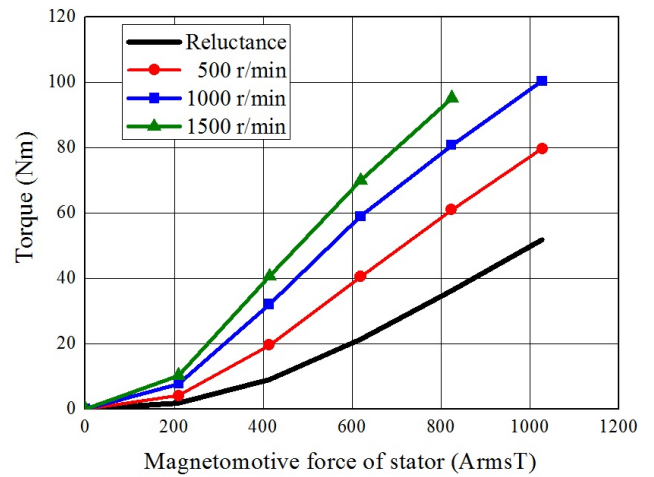


Fig. 14. Max torque with respect to magnetomotive force of stator.

## V. EXPERIMENTAL TEST RESULTS

The rotor induced current in the diode forward direction and the reverse direction for one pole pair is measured with a slip ring to demonstrate the self-excitation by the third space harmonic. Figure 12 shows the stator armature current (U-phase) and rotor current waveforms (induced and field current) for 500 r/min under 414  $A_{rms}T$  and 2000 r/min under 414  $A_{rms}T$  of the stator armature magnetomotive force. The inverter carrier frequency is set at 10 kHz. In the experimental test, the load test of the motor is limited in the low speed range. By referring to rotor current waveforms in Fig. 12, the induced current flows forward and reverse at time intervals. Thus, it can be easily confirmed that the third time harmonic on the rotating reference frame (the second space harmonic on static coordinates) links to rotor windings and the electromagnet poles can be obtained by field current generated with full-bridge rectifier as shown in Fig. 3. The adjustable speed drive characteristics with respect to current phase under armature magnetomotive force 210  $A_{rms}T$ , 414  $A_{rms}T$  and 620  $A_{rms}T$ , which is shown in Fig. 13, of proposed diode-rectifier magnet-free motor is investigated by controlling speed at a bench, and controlling torque with inverter. Figure 14 shows max torque (MTPA control point) with respect to magnetomotive force. As shown in Fig. 13 and Fig. 14, it can be confirmed that the additional torque by the E-coils greatly contributes to increase the total output torque with respect to rotation speed increase. The proposed motor is able to use the electromagnet torque in addition to conventional torque, i.e., a magnet torque and a reluctance torque. When the fundamental frequency is higher, the total torque shows a characteristic to increase because the time rate of change of the magnet flux linked to rotor winding is increase. Thus, the induced voltage to a rotor windings by Faraday's law, as a results, induced current increase, and electromagnet torque increase.

## VI. CONCLUSION

This paper has presented a rare-earth-free synchronous motor where space harmonic power is utilized for field magnetization instead of permanent magnets. The effect of

the auxiliary poles placed on the  $q$ -axis has analytically discussed. In addition, it has been presented that the torque density comparable with the conventional IPMSM can be achieved by the proposed rare-earth-free technique through the FEM based computer simulations. Furthermore, verification of the self-excitation principle generated by the space harmonics power has been demonstrated through the experimental test results. The future work of this study is to clarify the effects of the auxiliary poles and to reveal the efficiency of the proposed motor. On the other hand, the proposed motor has disadvantages due to the low torque density in the extremely low speed range. The authors have already suggested the effective solution in the computer simulation[18]. The idea of flux-intensifying control with time harmonic injection using pulse current command during effective periods will be experimentally verified. It is also important to develop the more accurate mathematical model since estimation of the induced current and the field current of the rotor windings is significantly important for the proposed motor.

#### REFERENCES

- [1] Y. Sato, S. Ishikawa, T. Okubo, M. Abe and K. Tamai, "Development of High Response Motor and Inverter Ssystem for the Nissan LEAF Electric Vehicle," *SAE Technical Paper* 2011-01-0350, 2011.
- [2] C. Pollock, H. Pollock, R. Barron, J.R. Coles, D. Moule, A. Court and R. Sutton, "Flux Switching Motors for Automotive Applications," *IEEE Trans. I.A.*, vol. 42, No. 5, pp. 1177-1184, 2006.
- [3] T. Kosaka, N. Matsui, Y. Kamada and H. Kajiura, "Experimental Drive Performance Evaluation of High Power Density Wound Field Flux Switching Motor for Automotive Applications," *The 7th IET Int. Conf. on Power Electronics, Machines and Drives (PEMD)*, B8.01-0418, 2014.
- [4] S. Nonaka, K. Kesamaru, "Brushless Self-Excited Single-Phase Synchronous Generator Using Wound Rotor Type Three-Phase Induction Machine," *IEEJ* vol. 101, No.6, pp.743-750, 1981
- [5] S. Nonaka, "The Self-Excited Type Single-Phase Synchronous Motor," *IEEJ Trans.*, vol. 78, No. 842, pp. 1430-1438, Nov. 1958. (in Japanese)
- [6] S. Nonaka, "The Brushless Self-Excited Type Single-Phase Synchronous Generator," *IEEJ Trans.*, vol. 82, No. 883, pp. 627-634, Apr. 1962. (in Japanese)
- [7] S. Nonaka and I. Muta, "An Analytical Study of the Brushless Self-Excited Type Single-Phase Synchronous Generator," *IEEJ Trans.*, vol. 86, No. 934, pp. 1140-1149, Jul. 1966. (in Japanese)
- [8] T. Fukami, Y. Hanada and T. Miyamoto, "Analysis of the Self-Excited Three-Phase Synchronous Generator Utilizing the 2nd-Space Harmonic for Excitation," *IEEJ Trans. I.A.*, vol. 117, No. 1, pp. 57-65, 1997. (in Japanese)
- [9] M. O. Oliveira, A. S. Bretas, F. H. Garcia, L. A. Walantus, H. E. Munoz, O. E. Perrone and J. H. Reversat, "Design and Analysis of Brushless Self-Excited Three-Phase Synchronous Generator," *International Conference on Renewable Energies and Power Quality (ICREPQ12)*
- [10] S. Li, B. Yuan, "Study on a Novel Brushless Self-Excited and Three-Phase Synchronous Generator with Constant Voltage Output," *2012 International Conference on Electrical and Computer Engineering (ICECE2012)*, 978-1-61275-029-3, pp. 47-52 (2012)
- [11] L. F. A. Izzat, S. Heier, "Development in Design of Brushless Self-Excited and Self-Regulated Synchronous Generator," *The 2nd International Conference on Renewable Energy Research and Applications (ICRERA)*, ID374, 2013.
- [12] J. Oyama, S. Toba, T. Higuchi and E. Yamada, "The Principle and Fundamental Characteristics of Half-Wave Rectified Brushless Synchronous Motor," *IEEJ Trans. I.A.*, vol. 107, No. 10, pp. 1257-1264, 1987. (in Japanese)
- [13] J. Oyama, T. Higuchi, N. Abe, and E. Yamada, "The Principle and Fundamental Characteristics of AC-Excited Brushless Synchronous Motor," *IEEJ Trans. I.A.*, vol. 109, No. 7, pp. 515-522, 1989. (in Japanese)
- [14] G. Dajaku, D. Gerling t, "New Self-Excited Synchronous Machine with Tooth Concentrated Winding," Document of university of Muenchen
- [15] K. Hiramoto, H. Nakai, E. Yamada, N. Minoshima and M. Seguchi, "Rotary Electric Machine and Driving Controller for Rotary Electric Machine," US20100259136 (Published in 2010)
- [16] K. Hiramoto, H. Nakai, "Propoosal and Feasibility Study of the Integrated Diode Synchronous Motor," *IEEJ Annual Meeting*, No. 5-054, pp. 97-98, 2014. (in Japanese)
- [17] K. Hiramoto, H. Suzuki, H. Nakai, E. Yamada, R. Mizutani, N. Minoshima, "Increment of the Integrated Diode Synchronous Motor in the Low Revolution Speed Area," *IEEJ Annual Meeting*, No. 5-055, pp. 99-100, 2014. (in Japanese)
- [18] M. Aoyama, T. Noguchi, "Preliminary Study on Rare-Earth Free Motor with Field Pole Excited by Space Harmonics," *IEEJ Annual Meeting*, No. 5-051, pp. 91-92, 2013. (in Japanese)
- [19] M. Aoyama, T. Noguchi, "Estimation of Rotor Current on Mathematical Model of Wound-Field Synchronous Motor Self-Excited by Space Harmonics," *The 22nd International Symposium on Power Electronics, Electrical Drives, Automation and Motion (Speedam)*, EMD0058, pp.589-594, 2014.
- [20] M. Aoyama, T. Noguchi, "Torque Performance Improvement with Modified Rotor Winding Circuit of Wound-Field Synchronous Motor Self-Excited by Space Harmonics," *IEEJ Trans. I.A.*, vol. 134, No. 12, pp. 1038-1049 (in Japanese).
- [21] M. Aoyama, T. Noguchi, "Preliminary Study on Active Magnetization Control of Rare-Earth Free Motor with Field Poles Excited by Space Harmonics," *IEEJ Technical Meeting*, MD-13-035, RM-13-044, 2013. (in Japanese)